HHS Public Access

Author manuscript

J Magn Reson. Author manuscript; available in PMC 2018 January 01.

Published in final edited form as:

J Magn Reson. 2017 January ; 274: 137–143. doi:10.1016/j.jmr.2016.11.015.

Saturation-Inversion-Recovery: a Method for T_1 Measurement

Hongzhi Wang[1,2,3], **Ming Zhao**[3,4], **Jerome L. Ackerman**[3,5], and **Yiqiao Song**[3,6]

[1]Shanghai University of Medicine and Health Science, Shanghai 200093 China

[2]Shanghai Key Laboratory of Magnetic Resonance, East China Normal University, Shanghai 200062 China

[3]Athinoula A. Martinos Center for Biomedical Imaging, Department of Radiology, Massachusetts General Hospital, Charlestown, MA 02129 USA

[4]Department of Physics, University of Massachusetts Lowell, Lowell, MA 01854 USA

[5]Harvard Medical School, Boston, MA 02115 USA

[6]Schlumberger-Doll Research, Cambridge, MA 02143 USA

Abstract

Spin-lattice relaxation (T_1) has always been measured by inversion-recovery (IR), saturation-recovery (SR), or related methods. These existing methods share a common behavior in that the function describing T_1 sensitivity is the exponential, e.g., $\exp(-\tau/T_1)$, where is the recovery time. In this paper, we describe a saturation-inversion-recovery (SIR) sequence for T_1 measurement with considerably sharper T_1-dependence than those of the IR and SR sequences, and demonstrate it experimentally. The SIR method could be useful in improving the contrast between regions of differing T_1 in T_1-weighted MRI.

Graphical abstract

Correspondence to: Hongzhi Wang.

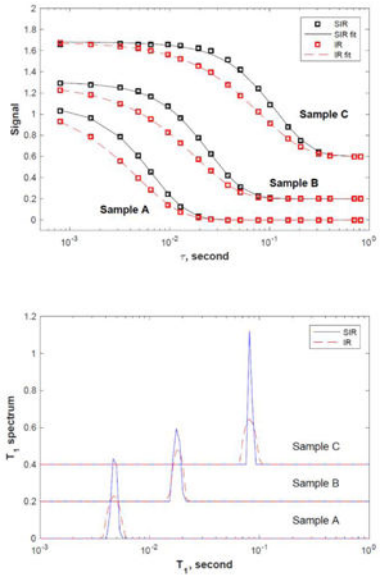

The inversion results show that both the IR and SIR methods yield the same T_1 value of 4.5 ms (sample A), 17 ms (sample B) and 79 ms (sample C), respectively. The SIR spectra are very similar to the IR ones but are noticably sharper.

Keywords

spin-lattice relaxation; saturation inversion recovery; T_1 contrast; T_1 dispersion

1. Introduction

For many years, spin-lattice relaxation has always been measured by inversion-recovery (IR), saturation-recovery (SR), or related methods [1-3]. However, it is known that the resolution in T_1 is limited in such measurements [4-6]; it can be challenging to reliably discriminate between T_1 values less than half an order of magnitude apart. Better signal-to-noise ratio (SNR) may improve the discrimination between T_1 values with the downside of longer acquisition times [7-10].

The primary reason for such lack of T_1 resolution is that the magnetic resonance (MR) signal dependence on the relevant recovery time (recycle delay or inversion time) is smooth, not sharp [5-6]. For the saturation-recovery experiment, the signal K_{SR} at a recovery time τ is:

$$K_{\mathrm{SR}}(\tau, \mathrm{T}_1)=1-\exp\left(-\frac{\tau}{\mathrm{T}_1}\right) \quad (1)$$

This function describes the dependence of the signal on the experimental (τ) and material parameters (T_1) for a single T_1 value; we call this function the *kernel* of the experiment. For example, for τ = 1 s, the MR signal intensities corresponding to T_1s of 1 sec and 1.1 sec are

very close: within 6% of each other. If a mixed sample contains materials with multiple T_1 values, the signal will be the sum of all components $S_{SR}(\tau) = \Sigma_i f_i[1 - \exp(-\tau/T_{1i})]$, where T_{1i} is the T_1 value of the i-th component and f_i is the weight of the component.

An experiment with a sharper kernel could improve the discrimination among different T_1 components [5,6]. For example, if an experiment can be performed with the following kernel:

$$K(\tau, T_1)=[1 - \exp(-\tau/T_1)]^2=K_2, \quad (2)$$

then the signal difference between T_1 = 1 and 1.1 s is increased to 12%, thus better discriminating between the different T_1s. In fact, higher exponents, such as $K_5(\tau, T_1) = [1 - \exp(-\tau/T_1)]^5$, shown in Fig. 1, will make the kernel even sharper and further improve the discrimination between different T_1 values.

In this paper, we describe an experimental implementation of the K_2 kernel. We designed a pulse sequence which can perform the kernel K_2 and demonstrated it experimentally on a high field spectrometer.

2. Description of the pulse sequence and experiment

2.1 Saturation-inversion-recovery (SIR) sequence

The SIR sequence is the 3-pulse sequence: 90° - τ - 180° - τ - 90° - acquisition. It can be viewed as an additional 90° pulse added in front of the IR sequence or a 180° pulse inserted in the middle of the SR sequence. The SIR sequence combines saturation and inversion processes, hence the name saturation-inversion-recovery sequence (SIR).

2.2 SIR kernel

For the SR sequence, immediately after each 90° saturation pulse, the longitudinal magnetization is zero (assuming transverse magnetization has dephased completely). Then the magnetization after the delay time τ follows Eq. 1, 1 – A, where $A = \exp(-\tau/T_1)$. Thus measurement using a series of τ values generates the T_1 relaxation curve with signal recovery from zero to the thermal equilibrium value as shown in Figs. 2a and 2b. We define the thermal equilibrium normalized longitudinal magnetization equal to unity. For the IR experiment, after the 180° pulse, the magnetization is inverted and this magnetization decays from −A to zero. The recovery magnetization grows as 1 – A as τ increases; thus the total signal is 1 – 2A as shown in Figs. 2c and 2d. Such decay/recovery analysis is based on the coherent pathway formulism [11].

The SIR sequence adds a 90° pulse before the IR sequence as shown in Fig. 2e, with the corresponding magnetization evolution shown in Fig. 2f. After the first 90° pulse, the longitudinal magnetization grows as 1 – A. The 180° pulse inverts it to −(1 – A) which then decays during the second τ period as −(1 – A)A. During this second τ, a recovery magnetization grows as 1 – A. Thus the total signal is the sum of the two pathways:

$$K_{\mathrm{SIR}}=1-\mathrm{A}-(1-\mathrm{A})\mathrm{A}=1-2\mathrm{A}+\mathrm{A}^2=(1-\mathrm{A})^2. \quad (3)$$

2.3 Signal shape and coherence pathway phase cycling

Application of several RF pulses can create many coherence pathways and thus signals (some are echoes, e.g., for diffusion measurements) [5, 12-16]. With the 3-pulse sequence, 90°-180°-90°, 9 signals (5 echoes and 4 FIDs) should be created with 9 different coherence pathways. We denote the coherence pathway as [q_0-q_1-q_2-q_3]. q_0 is the state before first 90° pulse, so q_0 is the prepared state and therefore q_0 = 0. q_1, q_2, q_3 is the state after each of the 3 pulses, with q_3 referring to the acquisition; by convention q_3 = −1. There are 9 possible coherence pathways [17] listed in Table 1.

For SIR, only the 5th signal [0, 0, 0, −1] is to be detected. We designed a phase cycling scheme to remove the unwanted signals: ph_1 = [0° 90° 180° 270° 180° 270° 90° 0°], ph_2 = [270° 180° 90° 0°], ph_3 = ph_{rec} = [180° 270° 0° 90°]. Using this phase cycling, we observe a consistent signal phase for all τ values from very short (τ = 0.8 ms) through very long (τ = 2048 ms), demonstrating the selection the single coherence pathway.

2.4 RF pulse error correction

For the SIR sequence, RF pulse inaccuracy and off-resonance effects are considered here. Fig. 3 a illustrates the pulse sequence with imperfect pulses and Fig. 3b shows the resulting signals with the 90° pulses replaced with α_1 degree pulses, and the 180° pulse replaced by an α_2 degree pulse. Transverse magnetization and residual longitudinal magnetization from the previous repetition of the pulse sequence are neglected in this analysis. Immediately following the α_1 pulse a residual normalized longitudinal magnetization $\cos\alpha_1$ remains, and it will decay as $S'' = A\cos\alpha_1$ in the delay time τ where $A = \exp(-\tau/T_1)$. At the same time, another longitude magnetization will appear as $S' = (1 - A)$. Immediately following the α_2 pulse, S' and S'' are transferred to the inverse Z direction and then decay as $S_2 = S'A\cos\alpha_2$ and $S_3 = S''A\cos\alpha_2$ separately. Meanwhile, there will appear another longitudinal magnetization $S_1 = 1 - A$. Thus after the last acquired RF pulse, the amplitude of the signal should be the sum of S_1, S_2 and S_3, that is

$$S=1-(1-\cos\alpha_2)A-\cos\alpha_2(1-\cos\alpha_1)A^2. \quad (4)$$

To explore the consequences of inaccurate RF pulse lengths we define $C_1 = (1 - \cos\alpha_2)$ and $C_2 = -\cos\alpha_2(1 - \cos\alpha_2)$ such that the SIR signal may be expressed as

$$S_{\mathrm{SIR}}=1-C_1A+C_2A^2 \quad (5)$$

If $\alpha_1 = 90°$ and $\alpha_2 = 180°$, then $S_{SIR} = (1 - A)^2$ as given in Eq. 3. The T_1 relaxation curve should begin (at $\tau = 0$) with an amplitude of 0 if the pulses are perfect, and with an

amplitude $1 - C_1 + C_2$ if they are not. The variation of the terms C_1 and C_2 as well as the initial value of the relaxation curve are plotted in Fig. 4.

Fig. 5 shows the simulated SIR relaxation curves for several α_1 and α_2 values around 90° and 180°, respectively. The simulations clearly demonstrate that small errors in the initial 90° pulse result in changes in the T_1 relaxation curve while the effect due to the 180° pulse error is much smaller. This suggests that the use of a saturation pulse train for the initial pulse instead of a single 90° pulse could be advantageous.

3. Experimental Results and Discussion

In order to test the SIR sequence, we prepared water solutions of $CuSO_4 \cdot 5H_2O$ yielding different T_1 values. The concentrations of samples A, B, and C were 7.13%, 1.78% and 0.36% by weight, respectively. The experiments were performed on a Bruker BioSpin (Billerica, MA, USA) Avance II spectrometer interfaced to a Magnex 14T (600 MHz) 89 mm vertical bore magnet using a Bruker 5-mm solution probe. For measurements on mixed fluid samples, a Wilmad-LabGlass (Vineland, NJ, USA) 4.14-mm outside diameter spherical microcell insert was used to contain fluid 1, and the 5-mm NMR tube with 0.36 mm wall thickness to contain fluid 2. The outer and inner diameters of the microcell are 4.14 mm and 3.25 mm, respectively. Thus the sample volume inside the microcell was about 10% of total fluid for a coil length of 15 mm. For each sample, we carried out T_1 measurements with the IR and SIR sequences using 22 recovery time values ranging from 0.8 to 2048 ms. The results are shown in Fig. 6 for the single fluid samples and Fig. 7 for the mixed fluid samples. The lengths of the pulses were adjusted to 90° and 180° (about 10 and 20 μs) for each sample.

The top panel of Fig. 6 shows the signal amplitude $(S(\tau = \infty) - S(\tau))$ as a function of the recovery time τ, for samples A, B and C, respectively. $S(\tau = \infty)$ is chosen to be the signal at the longest $\tau = 2048$ ms for each sample. The IR data (red squares) is scaled by 1.8 in order to match the SIR data (black circles) for easy comparison. It is clear that the SIR decay is noticeably sharper than the corresponding IR decay for all samples. The lower panel shows the corresponding T_1 spectra obtained using the Fast Laplace Inversion (FLI) algorithm [18] with the regularization parameter chosen to be 0.0001 for all measurements. The inversion kernel for SIR is shown in Eq. 6 and the values of C_1 and C_2 are calibrated using the experimental data of sample A ($\alpha_1 = 84.6°$ and $\alpha_2 = 180°$) and used for all other samples.

The inversion results show that both the IR and SIR methods yield the same T_1 value of 4.5 ms (sample A), 17 ms (sample B) and 79 ms (sample C), respectively. The SIR spectra are very similar to the IR spectra but are noticably sharper.

We also performed measurements on samples of mixed T_1, such as A+B, A+C, and B+C, and the results are shown in Fig. 7. Similar to the data for the single-fluid samples, the SIR decay curves are much sharper than that for the IR experiment reflecting the different kernel. The SIR and IR spectra are shown in the same plot for each sample to allow easy comparison. All spectra show two peaks corresponding to the two fluids present in each sample. The large peak is due to fluid 2 in the 5-mm NMR tube while the smaller one is

from the fluid in the microcell. The signal ratio of the small-to-large peaks is found to be 8.0%, 7.6%, 9.1% from SIR, and 8.5, 8.3%, 8.2% from IR, for the three samples (AB, AC, and BC), respectively. It appears that the variation of the smaller peak signal is less in the IR measurement. Both IR and SIR are able to isolate the different peaks and the linewidths of the individual peaks are similar for the SIR and IR measurements.

The position of the large peak is very consistent between the two measurements (SIR and IR). On the other hand, the smaller peaks are slightly different for the SIR and IR measurements. For example, for sample AB, the T_1 value of the smaller peak is 3.1 ms for IR, and 3.5 ms for SIR. For sample AC, these values are 3.3 and 3.3 ms, and for sample BC, 11 and 15 ms, respectively. Comparing to the T_1 values obtained from the single fluid samples, the T_1 value of the smaller peak is less accurate in both SIR and IR measurements (SIR is slightly better). Such behavior (inaccuracy of the smaller amplitude signal in Laplace inversion) is expected [5].

Using theoretical analysis and experimentation, we demonstrate that the SIR approach for T_1 measurement exhibits a kernel very different from that of conventional IR and SR measurements and their variants. This difference is most highlighted in the time-domain signals where the SIR sequence provides a significantly sharper τ or T_1 dependence for both single-fluid samples and mixed-fluid samples. Such enhanced constrast could be used in measurements to better identify or detect sample constituents based on their T_1 values, for example in T_1-weighted MRI. In this scenario, enhanced T_1 contrast might be achieved by inserting an SIR magnetization preparation module into the imaging pulse sequence to impose differential saturation among tissues. To better illustrate this hypothetical example, Fig. 8 plots the signal ratio of brain white matter (taking $T_1 \sim 0.65$ s) and grey matter ($T_1 \sim 1$ s), demonstrating a clear superiority of SIR contrast (defined as normalized signal ratio less unity) compared to conventional SR.

When using Laplace inversion to obtain the T_1 spectrum, we observed a significant improvement of T_1 resolution in the single-fluid samples (single peak spectra). For the mixed 2-fluids samples where the difference of the T_1 values is large, both SIR and IR methods are able to separate the two peaks. Application of the SIR method to broad T_1 distributions (such as porous and biological samples) is ongoing.

As shown in Fig. 1, other functional forms, such as K_5, may provide even an sharper kernel than K_2 (K_{SIR}). The question is whether a pulse sequence can be constructed to obtain such kernels. One option is to extend SIR to apply more 180° pulses with the same spacing τ between them. For convenience, we name these sequences SIRN where N is the number of 180° pulses. The kernel for such an SIR sequence family can be written as:

$$K_{\mathrm{SIR}}^{N}(\tau, T_1) = \sum_{i=0}^{N} (-1)^i (1 - A) A^i. \quad (6)$$

For example, when N = 0, the sequence corresponds to saturation recovery; when N = 1, to SIR. For N = 2,

$$K^2_{\mathrm{SIR}}(\tau, T_1) = 1 - 2A + 2A^2 - A^3. \quad (7)$$

Fig. 9 (left panel) plots the first few kernels in this family with N = 0, 1 and 2. Interestingly, sequences with higher N do not become sharper; in fact, they fall between SR and SIR.

Singular value decomposition (SVD) is a useful approach to determine the quality of the kernels [5,6]. If a kernel is smooth, the singular values decay rapidly, indicating that the inversion is more ill-conditioned. Fig. 9 (right) plots the singular values of the three kernels showing that the decay of the singular values is slowest for SIR and fastest for SR, and therefore that the SIR kernel is less ill-conditioned than that of SR. The SIR2 singular values fall between SR and SIR, consistent with the picture from the τ dependence (Fig. 9 left).

4. Conclusion

This work reports the theory and experimental results of a T_1 measurement scheme that combines at least two different T_1 relaxation periods in the pulse sequence. This is quite different from traditional inversion-recovery and saturation-recovery. The traditional methods incorporate only one decay period, and thus the decay function is exponential. The SIR method changes the basic functional form of the relaxation decay and results in a noticeably sharper kernel, which can enhance discrimination between similar T_1 values. It is possible to further improve it by incorporating relaxation intervals with different durations. In addition to benefiting NMR studies of porous media and other materials with wide T_1 dispersion, this method could provide a significant improvement in T_1-weighted MRI to yield higher contrast among tissues.

Acknowledgments

The work was supported by the Special Project for the Major Scientific Instrument Grant from China National Ministry of Science and Technology 2013YQ170406. Spectrometer laboratory support was provided by the Martinos Center and NIH grants S10RR013026 and P41EB015896. We thank Drs. Sara Sprinkhuizen and Jeffrey Paulsen for informative discussions.

References

1. Kleinberg, R. Encyclopedia of Nuclear Magnetic esonance. Grant, DM.; Harris, RK., editors. Wiley; New York, USA: 1995.
2. Levitt, MH. Basics of Nuclear Magnetic Resonance. Wiley; Chichester, UK: 2001. Spin Dynamics.
3. Munn K, Smith DM. A NMR Technique for the Analysis of Pore Structure: Numerical Inversion of Relaxation Measurements. J Colloid Interface Sci. 1987; 19:117–126.
4. Kleinberg RL, Vinegar HJ. NMR properties of reservoir fluids. Log Anal. 1996; 37:20–32.
5. Song YQ, Venkataramanan L, Burcaw L. Determining the resolution of Laplace inversion spectrum. J Chem Phys. 2005; 122:104104. [PubMed: 15836306]
6. Song YQ. Resolution and uncertainty of Laplace inversion spectrum. Magn Reson Imag. 2007; 25:445–448.
7. Whittall KP, MacKay AL. Quantitative interpretation of NMR relaxation data. J Magn Reson. 1989; 84:134–152.
8. Parker R, Song YQ. Assigning uncertainties in the inversion of NMR relaxation data. J Magn Reson. 2005; 174:314–324. [PubMed: 15862250]

9. Prange MD, Song YQ. Quantifying uncertainty in NMR T_2 spectra using Monte Carlo inversion. J Magn Reson. 2009; 196:54–60. [PubMed: 18952474]
10. Levitt MH, Madhu PK, Hughes CE. J Magn Reson. 2002; 155:300–306. [PubMed: 12036341]
11. Sigmund EE, Caudal N, Song YQ. Rapid T_1 measurement via decay-recovery decomposition: applications in fringe field and distributed relaxation experiments. Solid State Nuclear Magn Reson. 2006; 29:232–241.
12. Natala I, Colan EH, Malcolm HL. Multiplex phase cycling. J Magn Reson. 2003; 160:52–58. [PubMed: 12565049]
13. Song YQ. Categories of coherence pathways for the CPMG sequence. J Magn Reson. 2002; 157:82–91. [PubMed: 12202136]
14. Borgia GC, Brown RJ, Fantazzini P. Uniform-penalty inversion of multi-exponential decay data ii. data spacing, T_2 data, systematic data errors, and diagnostics. J Magn Reson. 2000; 147:273–285. [PubMed: 11097819]
15. Bain AD. Coherence levels and coherence pathways in NMR. A simple way to design phase cycling procedures. J Magn Reson. 1984; 56:418–427.
16. Ollerenshaw J, McClung RE. Determination of NMR cogwheel phase cycle with XML. J Magn Reson. 2000; 143:255–265. [PubMed: 10729251]
17. Song YQ, Tang XP. A one-shot method for measurement of diffusion. J Magn Reson. 2004; 170:136–148. [PubMed: 15324767]
18. Song YQ, Venkataramanan L, Hürlimann MD, Flaum M, Frulla P, Straley C. T(1)-T(2) correlation spectra obtained using a fast two-dimensional Laplace inversion. J Magn Reson. 2002; 154:261–268. [PubMed: 11846583]

Highlights

- An improvement over conventional inversion-recovery (IR) or saturation-recovery (SR) spin-lattice relaxation time measurement is proposed.
- The new method, saturation-inversion-recovery (SIR), combines saturation and inversion to achieve better discrimination between closely spaced T_1 values.
- Experimental demonstration of SIR method showing the sharper signal decay for single and multi-components samples indicative of improved differentiation of T_1s.
- An analysis of flip angle errors in SIR measurement is provided.

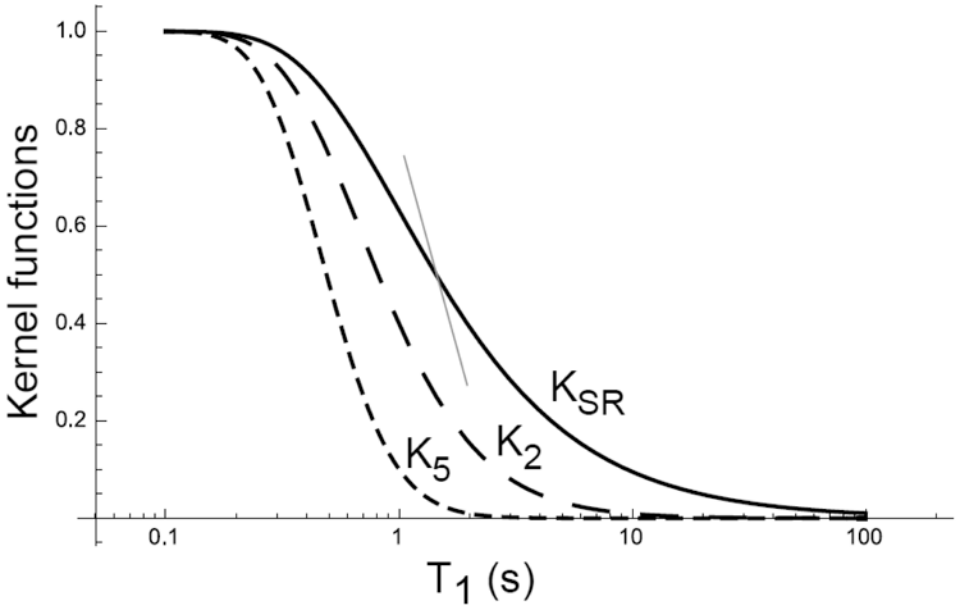

Figure 1.

Plots of the kernel K_n for SR and other potential kernel functions at $\tau = 1$ s. The solid curve for K_{SR} exhibits a gentle decay slope. The dashed and dotted curves represent K_2 and K_5, respectively, and exhibit progressively steeper slopes. The thin red line shows the slope of K_5 at $K_5 = 0.5$, displaced horizontally to intersect the curve for K_{SR} in order to highlight the difference between the two kernels.

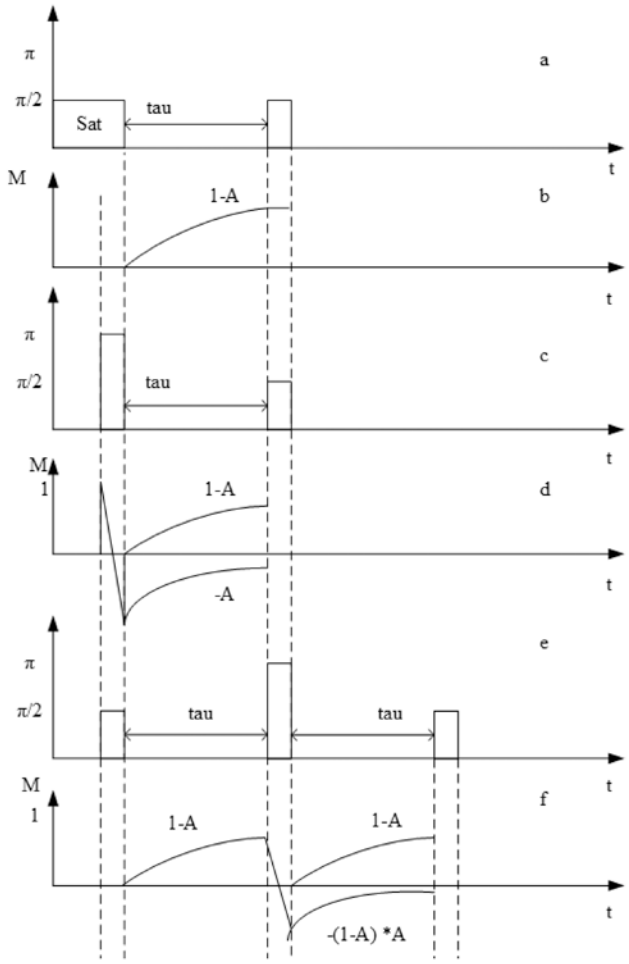

Figure 2.

The magnetization recovery pathways of the several T_1 sequences. (a) SR sequence diagram; (b) evolution of longitudinal magnetization in SR; (c) IR sequence diagram; (d) evolution of longitudinal magnetization in IR; (e) SIR sequence diagram; (f) evolution of longitudinal magnetization in SIR.

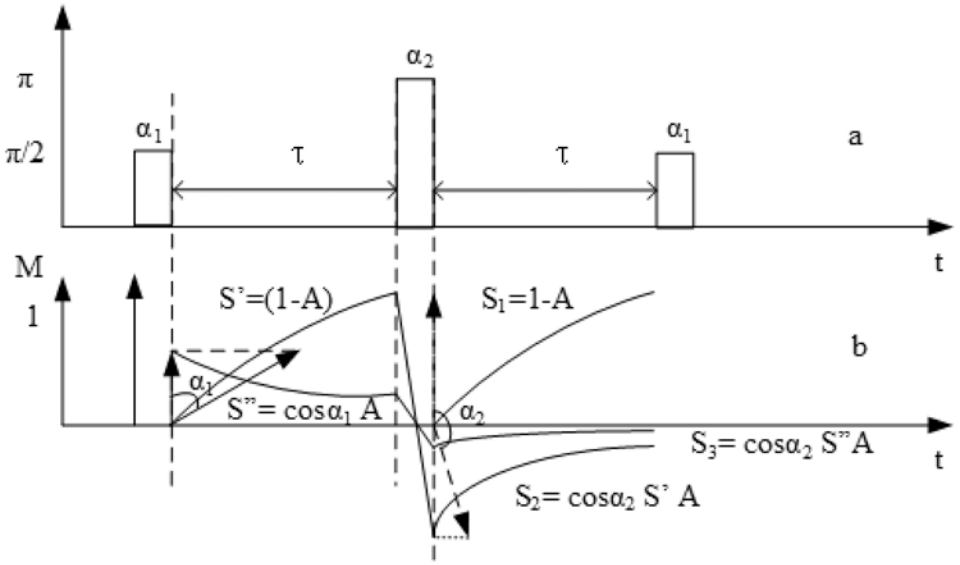

Figure 3.

Analysis of SIR sequence with imperfect RF pulses. (a) Sequence diagram; (b) Evolution of the longitudinal magnetization.

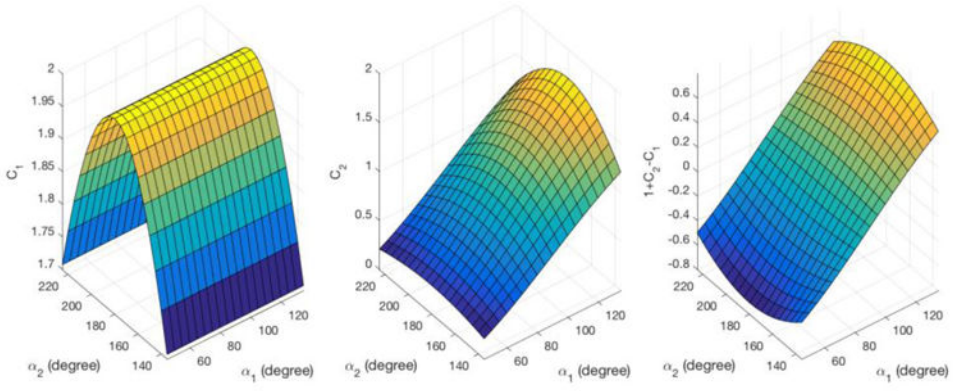

Figure 4.

The dependence of C_1, C_2 and the initial value of the SIR T_1 relaxation curve $1 – C_1 + C_2$ on the flip angles a_1 and a_2. Left: C_1 is strongly dependent on a_2 and independent of a_1. Center: C_2 is strongly dependent on a_1 and modestly on a_2. Right: the initial value of the T_1 curve exhibits a strong dependence on a_1 and a much weaker dependence on a_2.

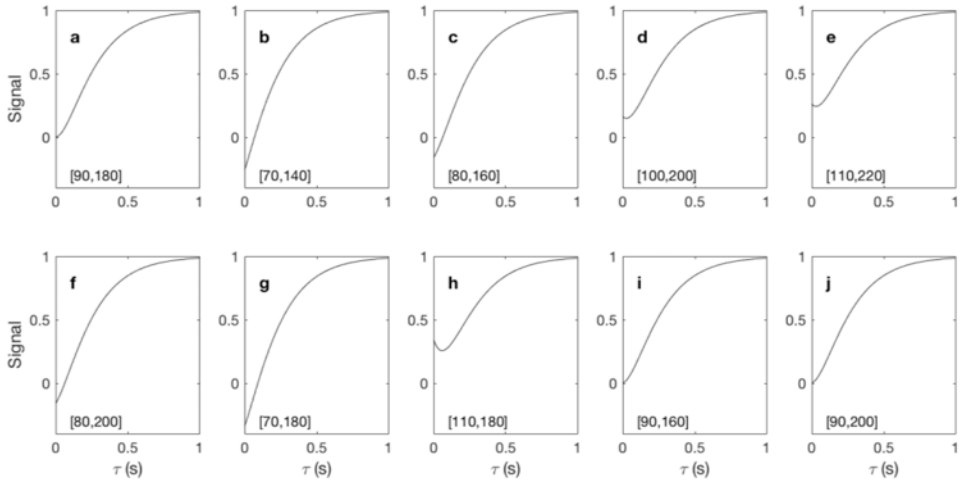

Figure 5.

Simulated T_1 recovery curve for different tipping angles of α_1 and α_2. (a-h) The [α_1, α_2] values (in degrees) are displayed in each panel. The T_1 value in this simulation is 200 ms.

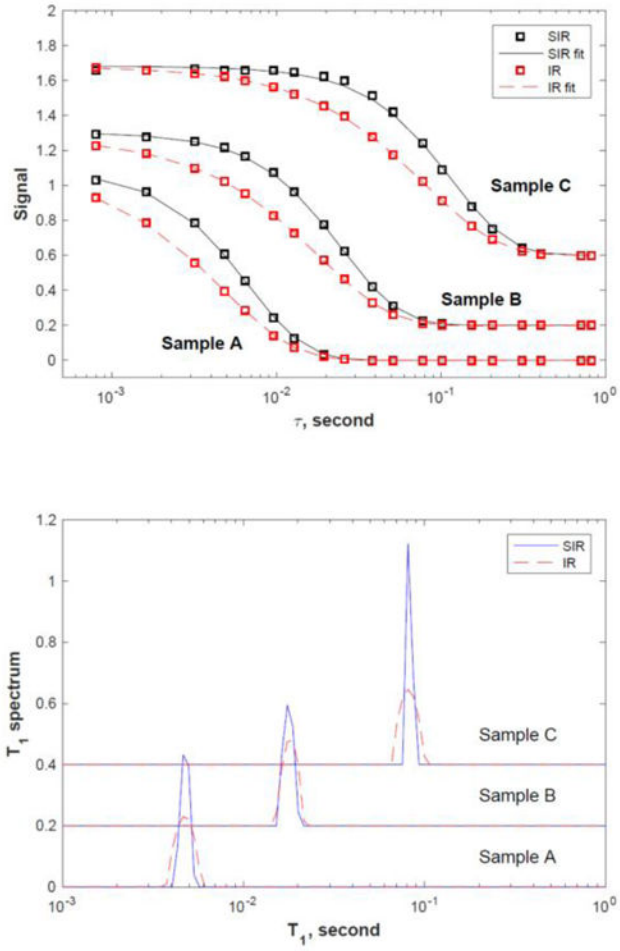

Figure 6.

Decay signal curves, $S(\tau = \infty) - S(\tau)$, (top panel, SIR: black circles, IR: red squares) and the corresponding T_1 spectra (bottom panel, SIR: solid line, IR: dotted line) for samples A (4.5 ms), B (17 ms), and C (79 ms). The lines in the top panel are fitting results from the Laplace inversion. The data for sample B and C in both panels are shifted upward for clarity.

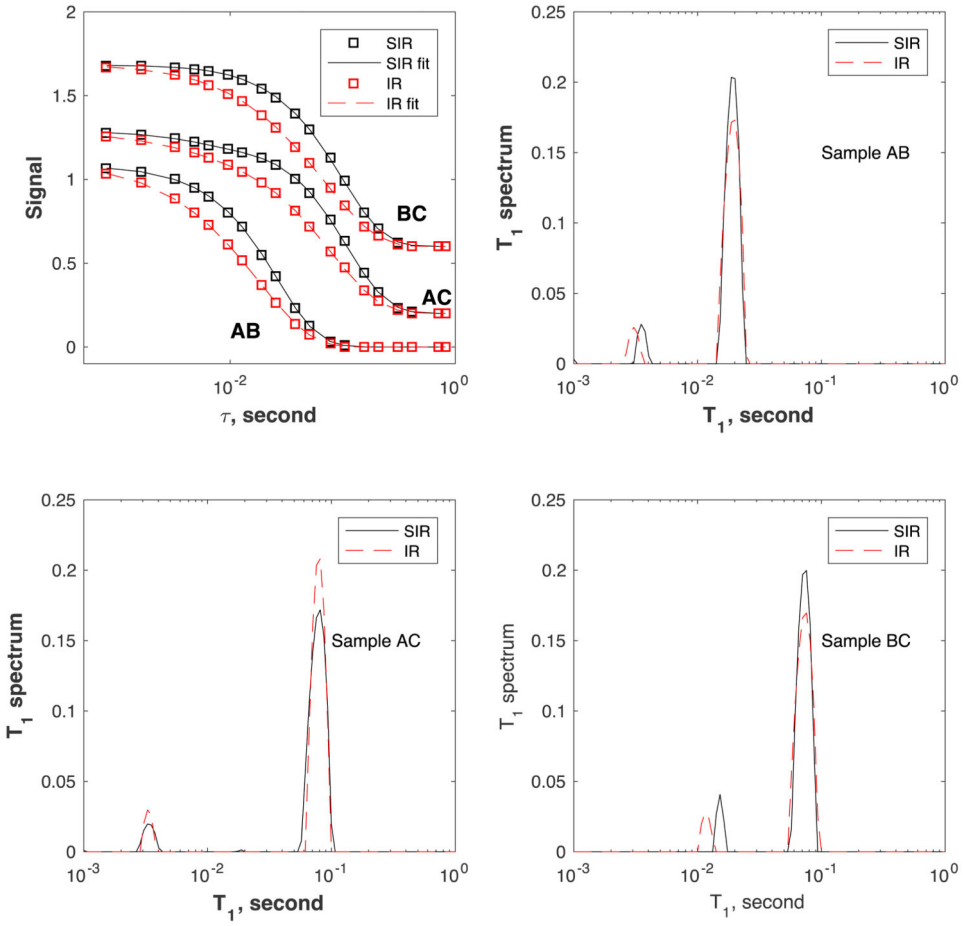

Figure 7.

Signal decay curves S($\tau = \infty$) – S(τ) (top-left panel, SIR: black circles, IR: red squares) and corresponding T_1 spectra (right and bottom panels, SIR: solid line, IR: dotted line) for the mixed samples AB, AC, and BC. The lines in the top-left panel are fitting results using the Fast Laplace inversion algorithm [18]. The data for samples AC and BC in the top-left panel are shifted upward for clarity.

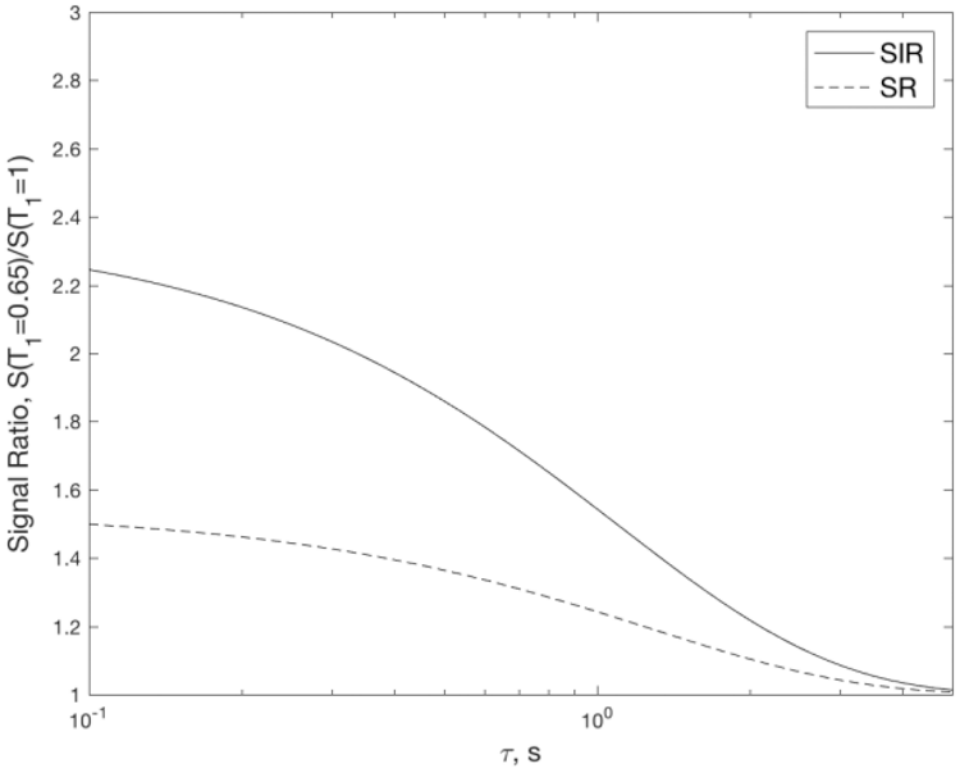

Figure 8.

Ratio of signals with T_1 = 0.65 s and 1 s as a function of the recovery time τ for SIR (solid line) and SR (dashed line) sequences. The higher value for SIR shows an improved contrast between the different T_1 values. For example, at τ = 0.65 s, SIR achieves more than twice the contrast (defined as normalized signal ratio less unity) of SR.

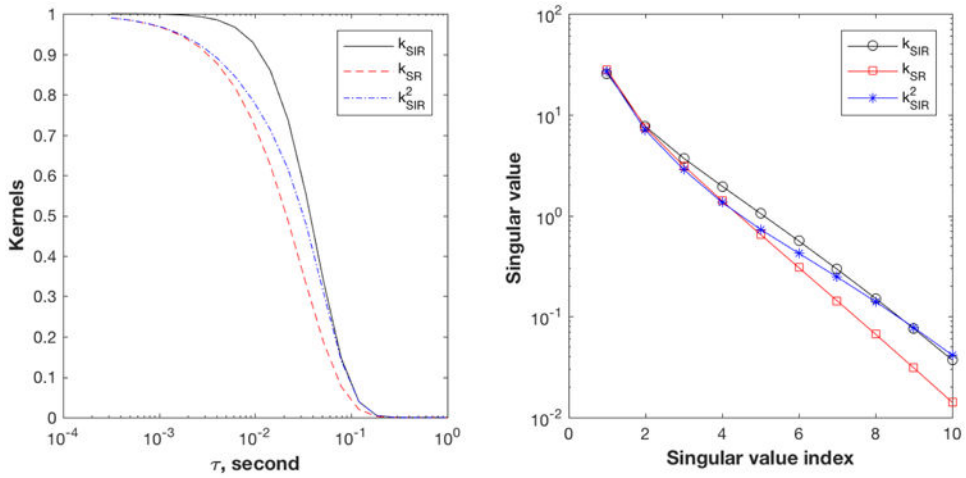

Figure 9.

Comparison of kernels of SIR family sequences. SIR (solid line), SR (red dashed line) and SIR2 (blue dash-dotted line). Left: Signal decay curves for T_1 = 0.03 s for the three sequences. Right: Plot of the singular values of the three kernels. The kernel matrices are evaluated as $K(\tau, T_1)$ with 20 τ values from 0.3-1000 ms, and 100 T_1 values from 1-1000 ms. SVD is calculated using MATLAB (Mathworks, Natick MA).

Table 1

Coherence pathways of SIR

Pathway	q_0	q_1	q_2	q_3
1	0	-1	-1	-1
2	0	-1	0	-1
3	0	-1	1	-1
4	0	0	-1	-1
5	0	0	0	-1
6	0	0	1	-1
7	0	1	-1	-1
8	0	1	0	-1
9	0	1	1	-1